Catalytic valorisation of the effluents generated during the defibrillation process of cellulose from almond hulls: A holistic zero-waste biorefinery approach

E. Frecha [a], J. Remón [a], A.P. Sulaeman [b], A.S. Matharu [c], I. Suelves [a], J.L. Pinilla [a,*]

[a] *Instituto de Carboquímica, CSIC, C/ Miguel Luesma Castán 4, 50018, Zaragoza, Spain*
[b] *Department of Chemistry, Faculty of Mathematics and Natural Science, Universitas Padjadjaran, Indonesia*
[c] *Green Chemistry Centre of Excellence, University of York, Department of Chemistry, Heslington, York, YO10 5DD, UK*

ABSTRACT

The acid-free hydrothermal microwave–assisted selective scissoring (Hymass concept) of cellulosic substrates is gaining keen interest in the field of materials science. Besides, implementing catalytic methodologies to upgrade side streams produced during this process could contribute to better, holistic utilisation of the starting feedstock. This work depicts a zero-waste biorefinery concept based on cellulose defibrillation from almond hulls using various hydrotreatment technologies (hydrogenation and hydrodeoxygenation) for downstream processing on a ruthenium catalyst. Therein, the hemicellulose separated from the biomass preconditioning step was converted into sugar alcohols and/or marketable polyols with a relatively high yield (47.4%) by hydrolytic hydrogenation (437 K, 3h, 5.0 MPa H$_2$). Meanwhile, a family of bioactive compounds (3-hydroxypyridines) could be directly extracted from the hydrolysate stream derived from microwave digestion, along with an energy carrier that was chemically stabilised (503 K, 60 min, 4.0 MPa H$_2$) to obtain fuel additives (diethyl succinic acid, DES) and/or fuel intermediates.

1. Introduction

Delivering chemicals and materials from biogenic renewable resources (i.e., lignocellulose biomass) has spread in the scientific community as a key resort for a future sustainable economy (Arevalo-Gallegos et al., 2017; Huber et al., 2006; Cherubini, 2010). Whereas a vast number of schemes for biomass valorisation focus on depolymerizing cellulose into its monomeric units followed by sugars conversion into a diverse range of products (Bhaumik and Dhepe, 2015; Bozell and Petersen, 2010), the complex molecular assembly of cellulose, defined by extensive intra- and inter-molecular H-bonds between glucose chains, often imposes many catalytic challenges for its efficient transformation, particularly under heterogeneous conditions (Geboers et al., 2011). In such a context, cellulose and modified cellulose retaining its innate structure arise as interesting materials, either a standalone product or blended (Zinge and Kandasubramanian, 2020; Lee et al., 2014). The remarkable stiffness and mechanical strength, as well as other notable genetic traits such as degradability, lightness, and minimal thermal expansion coefficient, have engendered innovative prospects for the use of cellulose crystals in novel applications upon their separation from the amorphous fraction and subsequent downsizing to the nanoscale. (Dufresne, 2013; Moon et al., 2011; Klemm et al., 2011). This kind of nanometric cellulose is raising attention in many practices like papermaking, environmental remediation, food packaging and biomedical industry. Also, the high aspect ratio with numerous phenolic groups provides an ideal scaffold for chemical modification, leading to a large portfolio of cellulosic derivatives (Sheikhi and Karak, 2019).

The hierarchical architecture of cellulose allows its breakage into an assortment of morphologies, involving microfibrils, nanofibrils or nanocrystals (Nelson et al., 2016). Cellulose nanocrystals are described according to the TAPPI W13021 standard nomenclature as highly crystalline particles in a rod-like shape, whereas cellulose nanofibres are elongated segments that alternate amorphous regions between crystalline domains (Kargarzadeh et al., 2018). Typically, elementary fibrils are isolated by shear forces, while acid treatments yield cellulose nanocrystals or whiskers (Xie et al., 2018). At the same time, various chemical and/or enzymatic methods have been developed and applied before the disintegration step to limit the energy inputs and/or facilitate

---

Notation		HHV	Higher Heating Value
		HPLC	High-Performance Liquid Chromatography.
ATR-IR	Attenuated Total Internal Reflectance Infrared Spectroscopy	ICP-OES	Inductively Coupled Plasma-Optical Emission Spectroscopy
B-1	Biomass pre-treated	MFC	Microfibrillated Cellulose
DES	Diethyl Succinic acid	MW	microwave
DOD	Degree of Deoxygenation	MW-HT	Microwave Hydrothermal Treatment
E-1A	stream derived from E-1 once it was re-dissolved in water	NIST	National Institute of Standards and Technology
E-1	liquour derived from the pretreatment stage (ethanolsolv process)	OP-A:	Organic phase extracted from the effluent E-2 using ethyl acetate as the sole extracting reagent
E-2	liquour derived from the MW-hydrothermal treatment	OP-B:	Organic phase extracted from the effluent E-2 using ethyl acetate and chloroform as extracting reagents
EtOAc	Ethyl acetate	RT	Room Temperature
FID	Flame Ionisation Detector	TAPPI	Technical Association of Pulp and Paper Industry
GC/MS	Gas Chromatography (GC) coupled to Mass Spectrometer (MS)	TEMPO	2,2,6,6-tetramethylpiperidine-1-oxyl radical

the release of individualised fibrils. Some of these procedures include pulping and bleaching, steam explosion, acid, alkaline or enzymatic hydrolysis, or the introduction of charged groups via carboxymethylation or 2,2,6,6-tetramethylpiperidine-1-oxyl radical (TEMPO)-mediated oxidation (Xie et al., 2018; Jonoobi et al., 2015). However, using such pre-treatments is usually time-consuming, while employing chemical reagents causes waste disposal issues and overall high expenses (Xie et al., 2016). Another concern of these methods is that they degrade the C5/C6 fraction of hemicellulose, with a deleterious impact on carbon efficiency. Therefore, further advances in biomass defibrillation in terms of cost, time-efficiency or environmental viewpoint are worth being sought.

In this particular context, a viable eco-friendly solution lies in the hydrolysis of amorphous cellulose regions in subcritical water. The utilisation of pure water as the single hydrolysing agent enables optimal diffusion conditions in a system that is environmentally sustainable (i.e., free of any additives, non-corrosive, and discharging less harmful effluents). (Novo et al., 2016). By these means, Novo et al. managed to degrade various cellulosic substrates at 393 K and 20.3 MPa into nanocrystals with a total yield of 21.9% within 60 min (Novo et al., 2015). Later, de Melo et al. reported a state-in-the-art hydrothermal microwave-assisted selective scissoring (Hymass) method to produce simultaneously cellulose nanocrystals and (meso)porous fibrils from orange peel residues after only 15 min of reaction at relatively mild temperatures (393–493 K) (de Melo et al., 2017). Shortly afterwards, the use of microwave (MW) energy for the synthesis of nano-sized celluloses was spanned to a wide scope of origins: bamboo (Xie et al., 2016), citrus (Matharu and de Melo, 2018), ginger (Gao et al., 2021a), pea haulm (Gao et al., 2019), banana stems (Iliyin et al., 2021), peel or bracts (Harini et al., 2018) and so forth. These publications evidenced that the feedstock nature, process conditions and pre-treatments have a strong impact on the yield and final product properties. A critical parameter is the nanocellulose yield, which is mainly dictated by the fibre content in the substrate and reaction severity. Whereas rapid treatments may cause negligible hydrolysis effect, prolonged contact times or extremely high temperatures may prompt the dissolution of cellulose and the total degradation of its structure (polymorph conversion). Likewise, many other attributes like crystalline degree, morphology, and mechanical and thermal behaviours are heavily determined by the extracting method and source-dependency (Lavoine et al., 2012), making mandatory the assessment of bespoke processes to produce cellulose nanomaterials as per the raw material and the target-specific properties.

Very recently, Sulaeman et al. addressed the synthesis of microfibrillated celluloses (MFC) through the hydrothermal MW-processing of two alternative feedstocks: almond hulls and cassava peel (Sulaeman et al., 2021). Their work provided a rapid and facile preparation method for cellulose defibrillation from non-edible resources. Although this study marked the first step for the extensive and controlled production of MFC from almond hulls, the long-term success of this technology not only requires the integration of energetically efficient proposals, such as microwave heating, but also it is paramount to attain optimal recovery and valorisation of all side streams garnered from the process.

Several biorefinery concepts may be referred to illustrate plausible chemicals and energy co-production opportunities arising from a baseline process (Wyman, 2003). A benchmark process is the wood paper industry, where the spent cooking liquors are used for on-site cogeneration systems to produce steam and electricity or as a source of added-value chemicals (Reddy and Yang, 2005). For instance, many Kraft pulp mills collect certain extractives, such as turpentine and tall oil, to get an extra value for these streams (NagyKim et al., 2006). Some other options that could be beneficially integrated within the Kraft pulp manufacturing include the lignin recovery from the black liquor or the black liquor gasification to yield synthesis gas (Jönsson et al., 2013). Another timely and interesting option is the hemicellulose extraction prior to cooking for separate valorisation or recovering high-purity tannins from incidental wastes such as bark (Bozell and Landucci, 1993).

Following a similar work path, many other schemes could be devised to enlarge the range of products in modern-day biorefinery concepts and forthcoming commercial revenues (Konwar et al., 2018). In order to estimate the impact that different configurations may have on the biorefinery profits margin, Zhang et al. employed the synthesis of ethanol from corn stover as a case study for discussion. An economic evaluation based on the product incomes revealed that the sole production of ethanol and chemicals from sugars, alongside the lignin utilisation as burning fuels, could bring money returns up to $145 per ton of biomass. Instead, the entire transformation of biomass constituents into an array of marketable products (ethanol from glucose, added value compounds from xylose and other minor sugars, lignin-derived polymers and acetic acid as a commodity) could raise the net margin up to 6.2 fold ($641/ton) (Zhang, 2008). These numbers strongly incentivise exploring innovative biorefinery schemes based on defibrillated cellulose production that maximise resource utilisation through a meaningful combination of various conversion and extraction techniques for new stream applications.

To advance in this direction, the present study presents an innovative conceptual process design for the valorisation of intermediates and side streams extracted from the defibrillation of almond hulls, utilising sustainable chemical pathways. This marks the first time such a design has been proposed. Specifically, a supported ruthenium catalyst was applied on different catalytic hydrotreatments (hydrogenation and hydrodeoxygenation) to simultaneously produce sugar alcohols, bioactive extractable compounds (3-hydroxypyridines) and a biomass-derived organic oil (bio-oil). Sorbitol and xylitol are potential precursors for the synthesis of alkanes, aromatics or hydrogen (Luterbacher et al.,

2014), while the organic bio-oil can be further deoxygenated into bio-fuels and/or serve as a source of fine chemicals.

2. Experimental

Earlier, the optimal experimental conditions for the production of defibrillated nanocellulose from almond hulls were outlined (Sulaeman et al., 2021). The best-suited process conditions were established at 493 K (microwave irradiation time of 30 min), including an organosolv pre-treatment in ethanol. In this follow-up study, various catalytic hydrothermal methodologies (hydrogenation and hydrodeoxygenation) were interconnected with proper separation and refining stages and annexed to the main product line for effluent management. The flow sheet diagram of the process is schematically depicted in Fig. 1 and explained in detail in the following paragraphs.

2.1. Raw material and sample preparation

Almond hulls (Marcona variety) were harvested in 2019 from local farmland (Ricla, Zaragoza, Spain). First, the raw material was sterilised by ethanol-spraying (96 vol %, Panreac) and left under air-dry conditions. The sterilised sample was ground to a fine powder using, in sequence, a knife grinder (Retsch™ GM 300, 2500 rpm) and a coffee mill and finally sieved.

A flowchart of this work-up procedure can be found in Fig. S1. The compositional analysis of this biomass revealed a large fraction of carbohydrates (12.6 and 19.4% of cellulose and hemicellulose, respectively) and a relatively low content in lignin (25.1%), making it an attractive feedstock for the development of carbohydrate-based nanomaterials. A more comprehensive physicochemical analysis of almond hulls has been recently reported (Remón et al., 2020) and is briefly recalled in Table S1.

2.2. Defibrillated cellulose production

2.2.1. Organosolv pre-treatment

A magnetically-stirred mixture of almond hulls (20 g) was soaked in ethanol (96 vol%, 100 mL) inside a round-bottom flask (250 mL) and refluxed. Two hours later, the suspension was filtered *in vacuo* to separate a solid material (biomass pre-treated, B-1) from the sugar-rich liquor (E-1). The liquid filtrate was generally vaporised to recycle ethanol, leaving the dissolved organic matter as a solid residue that was weighed and diluted in 194 mL of water. This water volume was calculated to keep the solid concentration of the resulting stream, here denoted as E-1A, similar to the E-2 effluent.

2.2.2. MW-assisted hydrolysis

The hydrothermal treatment was performed in a CEM Mars microwave reactor (CEM Corporation, US). In a typical procedure, 2.0 g of pre-treated almond hulls (B-1) were suspended in 40 mL of deionised water inside a closed reaction vessel (EasyPrep Plus®, Teflon, 100 mL) and placed onto the rotor tray of the microwave. The mixture was then treated at 493 K with a set ramp time of 30 min at a maximum power inlet of 600 W. After that, the slurry was cooled down and filtered. The filtrate operation separated an aqueous hydrolysate effluent (E-2) from an insoluble product, which was thoroughly rinsed with water, hot ethanol and acetone and finally dried. The remaining solid was measured gravimetrically and denoted as microfibrils of cellulose (MFC), alluding to the high fibre content. The product yield (Y_{MFC}) was determined as the mass percentage of MFC with respect to the initial biomass mass (Eq. (1)):

$$Y_{MFC} \ (\text{wt. \%}) = \frac{\text{mass of MFC (g)}}{\text{mass of dried biomass (g)}} \cdot 100 \qquad [\text{Eq. 1}]$$

The aqueous solution E-2 was stored at 277 K until use for further analysis and experimentation.

2.3. Downstream catalytic conversion technologies

The effluents E-1 and E-2 were used as inlet streams for the subsequent valorisation, i.e., synthesis of sugar alcohols via hydrolytic hydrogenation and catalytic hydrotreatment for chemical stabilisation. Both processes were carried out in a stainless steel autoclave (45 mL, Berghof Products, BR-40 series) fitted with a temperature controller
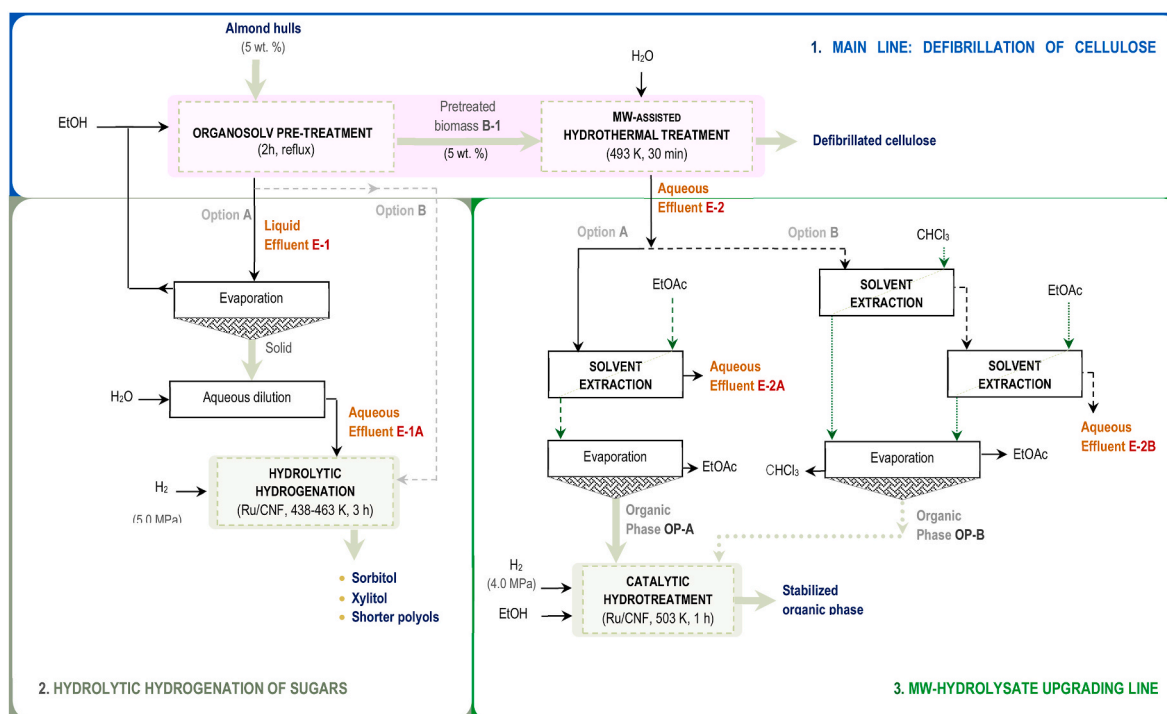

Fig. 1. Flow sheet diagram for cellulose defibrillation from almond hulls within a biorefinery approach.

(BTC-3000) heating jacket and magnetic stirrer. In addition, the two catalytic transformations were tested onto a catalyst based on ruthenium-supported carbon nanofibres (Ru/CNF) with proven hydrogenation activity for the hydrolytic hydrogenation of carbohydrates (Frecha et al., 2019). Further details about the catalyst characterisation and the experimental set-up can be found elsewhere (Frecha et al., 2019, 2021). Briefly, it was prepared according to the wet impregnation method with a nominal content of 0.5 wt % in Ru (actual metal loading of 0.38 ± 0.03 wt % defined by ICP-OES) and a mean crystallite size of 1.2 ± 0.2 nm (measured by Transmission Electron Microscopy).

2.3.1. Hydrolytic hydrogenation of sugars

The hydrolytic hydrogenations of E1 or E1-A (depending on the solvent) were conducted under various operational conditions, listed in Table 1. For this end, the effluent (20 mL) was introduced into the reaction vessel and combined with the required quantity of the Ru/CNF catalyst (1.4 g cat/g C). Such a dosage of catalyst corresponds to a catalyst to solid ratio equal to 0.5 by mass when the C content of the feedstock is considered by elemental analysis. After sealing, the reactor was evacuated and backfilled with N_2 and H_2 gas (three cycles) and then pressurised to 5.0 MPa of H_2 (measured at room temperature). Next, the system was heated to the desired temperature (438 or 463 K) and held stirred (1400 rpm) for 180 min. At the end of each test, the reactor was quenched in water and opened. At this point, the spent catalyst and solid products were separated by filtration, washed with deionised water, dried and finally weighed.

2.3.2. MW-hydrolysate upgrading line: organic phase extraction and mild hydrotreatment

The use of liquid organic solvents was explored as a means to valorise the hydrolysate stream E-2, affording a biomass-derived organic oil (bio-oil) with potential utility as an energy carrier and/or source of chemicals. To improve the quality of the extract, a consecutive catalytic hydrotreatment was applied. The effectiveness of this upgrading process was disclosed using a bio-oil sample obtained from thermochemical routes (MW-assisted pyrolysis) as a reference (See details in ESI).

The experimental conditions for the optimal extraction were assessed using ethyl acetate (EtOAc) as the sole solvent or a combination of chloroform ($CHCl_3$) and EtOAc through a successive extraction. The volume ratio of solvent to effluent was 2:1 for EtOAc and 1:1 for $CHCl_3$. The organic oil single extracted by a single solvent was labelled as OP-A, whilst OP-B refers to the extract obtained from the two-solvent methodology. In practice, the extraction was achieved in a separation funnel (100 mL) by adding the organic solvent to 30 mL of effluent. The mixture was vigorously shaken and decanted. Next, the organic phase was collected and replaced by an equal volume of fresh solvent. This operation was repeated three times. The liquids derived from each stage were mixed, and the produced extract was concentrated by evaporation (313 K, vacuum) and dried until constant mass.

The yield of the organic product was determined as the mass percentage (wt. %) of compounds retrieved from the aqueous to the organic phases, while the efficiency of the extraction was estimated by considering the carbon content in both fractions. In order to get enough amount of product and validate the experimental reproducibility, the extraction was performed at least in quadruplicate. Results correspond to an average value expressed as mean ± standard deviation.

The organic product extracted was partially deoxygenated in ethanol at an inlet H_2 pressure of 4.0 MPa. The results were compared to those obtained from the hydrodeoxygenation of a MW-pyrolysis oil. In these tests, 300 mg of bio-oil (OP or MW-pyrolysis oil) was dissolved in ethanol (20 mL, 96 vol %, Panreac) and mixed with the required amount of Ru/CNF catalyst to achieve a catalyst to bio-oil carbon ratio of 1.4 g cat/g C. The use of carbon ratios instead of a pre-fixed mass catalyst allows for a better comparison between samples with somewhat different C contents. Next, the reactor was purged and vented repeatedly, first with N_2 and then with H_2, and finally pressurised to 4.0 MPa H_2 (measured at room temperature). The treatment was performed at 503 K under magnetic stirring (1400 rpm) for 60 min, working at an effective pressure of 10.2 MPa. After that, the reaction was rapidly stopped by immersion in a tap water bath. The gas stream was collected for analysis prior to opening the reactor. Once it was opened, the liquid and solid phases were separated by vacuum filtration, rinsing the filter cake with ethanol until it became colourless. The soluble fraction was then dried in a two-step process, first in a rotary evaporator and then with N_2 gas to get the upgraded bio-oil. The formation of coke was estimated after subtracting the catalyst initial mass from the total amount of solid produced in the process on the assumption of no catalyst loss.

2.4. Product analysis

2.4.1. Characterisation of the aqueous phase

Liquid-phase products were quantitatively characterised by High-Performance Liquid Chromatography (HPLC) and Gas Chromatography (GC) coupled to a Mass Spectrometer (MS) and a Flame Ionisation Detector (FID). More details about the technical specifications of the instruments and measurement conditions can be found in the Electronic Supplementary Information (ESI). The product yields (Y) were determined on a carbon mass basis, taking into consideration the carbon contents of the products and the inlet effluent determined by elemental analysis (Eq. (2)):

$$Y\,(C-\%) = \frac{\text{weight of carbon in the product (g)}}{\text{weight of carbon in the inlet effluent (g)}} \cdot 100 \qquad \text{[Eq. 2]}$$

2.4.2. Characterisation of the gaseous stream

The gas phase volumetric composition was analysed by a Varian CP4900, Micro Gas Chromatograph (Micro-GC), with the following species quantified: CH_4, CO_2, CO and H_2.

2.4.3. Characterisation of the bio-oil and organic phase

The characterisation of the bio-oil included elemental and chemical compositions and higher heating values (HHV). The chemical composition was analysed by gas chromatography (GC/MS) using the same apparatus employed for the aqueous phase analysis and the NIST 05 spectral library for structural assignment. A semi-quantitative analysis, based on relative peak areas, was performed. The elemental composition (CNSH) was determined using a Thermo Flash 1112 Analyser, calculating the oxygen by difference. The HHV was theoretically estimated from the elemental analysis data using the empirical formula (Eq. 3) developed by Channiwala (Channiwala and Parikh, 2002):

$$HHV\,(MJ/kg) = 0.3491 \cdot C + 1.1783 \cdot H + 0.1005 \cdot S - 0.1034 \cdot O - 0.0151 \cdot N$$
$$\text{[Eq. 3]}$$

The degree of deoxygenation (DOD) was finally determined according to Eq. (4):

Table 1
Details of reaction conditions for each run.

Run	Solvent	Catalyst	H_2 pressure (MPa)[a]	Effective pressure (MPa)	Temp. (°C)	Time (h)
1	H_2O	–	5.0	8.0	165	3
2	H_2O	Ru/CNF	5.0	8.0	165	3
3	H_2O	Ru/CNF	5.0	9.0	190	3
4	EtOH	Ru/CNF	–	4.0	165	3
5	EtOH	Ru/CNF	5.0	6.9	165	3

[a] Measured at room temperature conditions.

$$DOD \text{ (wt. \%)} = \left(1 - \frac{\text{weight of oxygen in product (g)}}{\text{weight of oxygen in feed (g)}} \right) \cdot 100 \qquad \text{[Eq. 4]}$$

3. Results and discussion

The present work builds on an earlier study in which the experimental conditions for synthesising defibrillated cellulose from almond hulls were optimised. Under the umbrella of this process, a biorefinery approach was designed, in which all intermediates and side streams were considered within the overall strategy of valorisation to furnish different categories of products. The flowsheet of this research can be roughly organised around three main sections: i) pre-treatment and cellulose defibrillation, ii) hydrolytic hydrogenation of the sugar-rich liquid effluent produced during the pretreatment step (pre-microwave) and, iii) MW-hydrolysate upgrading line.

3.1. Main line: Pre-treatment and cellulose defibrillation

The extraction of cellulose microfibrils from almond hulls comprises a two-step procedure. First, the biomass is pre-soaked in ethanol to remove polar extractives. Monosaccharides, dimers and waxes are preferentially dissolved during this solvothermal approach and detached from the biomass. The second stage is the defibrillation of cellulose. The MW-assisted hydrothermal treatment is employed in the process to extract the cellulosic matter from the biomass matrix, consisting of remnants of hemicellulose, pectin, and lignin. Additionally, the treatment eliminates the amorphous regions of cellulose, resulting in a cellulose-rich material with a significantly high degree of crystallinity (61.5%). Herein, the application of MW irradiation results in the rapid internal heating of highly polar species (mainly carbohydrates), whereas substances like lignin with low polarity remain unheated. Such uneven distribution of temperatures within the biomass material, combined with the oscillation of polar parts to align with an electric field, was hypothesised that facilitate the separation and eventually disrupt their inter-twine structure (Hu and Wen, 2008; Li et al., 2014a; Gao et al., 2021b). At optimal MW-HT conditions (503 K, 30 min), bundles of needle-shaped micro cellulose fibrils with 4.0–4.3 nm in width and a few μm in length were attained in 33.4% yield (based on pre-treated biomass weight, B1). Since the removal of C5-C6 sugars densifies the ethanol-treated biomass, this yield corresponded to 27.8% of the total dry weight of almond hulls. Strictly speaking, the fibrous material obtained from this process ought to be designated as (ligno)cellulose microfibrils or defibrillated (ligno)cellulose, in reference to a product chiefly composed of cellulose, but still containing some residual lignin. The presence of lignin was concurrent with the mass product yield, which exceeded the anticipated theoretical value derived from the initial composition of almond hulls (12.6 wt % of cellulose). This fact was unambiguously verified by Attenuated Total Internal Reflectance Infrared Spectroscopy (ATR-IR) and 13C CPMAS NMR techniques in the preceding research (Sulaeman et al., 2021).

3.2. Hydrolytic hydrogenation of the sugar-rich effluent obtained in the pre-treatment step

The ethanosolv process, applied before the MW-hydrothermal treatment, not only enhances the physical properties of the final defibrillated nanocellulose but also results in an efficient fractionation of hemicellulose, which allows access for its straightforward valorisation into second-tier products and speciality chemicals that otherwise would be lost. The hemicellulosic matter was extracted from this stage in the form of soluble sugars, which were collected within the stream coded as E-1. On a mass basis, the overall yield of E-1 accounted for 16.8 wt% of the raw biomass. The ensuing analysis by HPLC determined xylose and glucose amounts of 24.6 and 18.4 C-%, respectively (based on the carbon content) and minor quantities of cellobiose (1.9 C-%) and lactic acid

(2.3 C-%). A meagre percentage of 1.5 C-% of sorbitol was also detected, likely forming part of the natural plant (Strain, 1937). The sum of these compounds amounted to ca. 41% of the hemicellulose initially present in the almond hulls (i.e., 19.4 wt %). Given the sugar richness of this stream, it was proposed for synthesising sugar alcohols by hydrolytic hydrogenation. For this purpose, various operational conditions (Table 1) were tested, with the product distribution of each run depicted in Fig. 2.

Firstly, the hydrolytic hydrogenation of E-1 was studied in the aqueous phase, i.e., vaporising E-1 to recycle the ethanol and re-solubilising the resultant solid to form the effluent E1-A. Undoubtedly, the high volatility of ethanol favours the solvent recovery by convectional distillation (Li et al., 2016). As this process could not solubilise the entire organic matter initially present in ethanol, a water-insoluble precipitate, accounting for 15.2% of C, was formed and separated by filtration. Afterwards, the soluble fraction was catalytically hydrogenated for 3 h at 438 K and 5.0 MPa of H_2 (RT) of pressure.

In the absence of a catalyst, only a negligible amount of sugar alcohols (merely 1.3%) was attained (blank test, Run 1), whereas a substantial degradation of sugars was noted, losing around 39.1% of the initial xylose and 16.0% of glucose. Meanwhile, the amounts of 5-HMF and other unwanted furan-based solid products (humins) increased commensurately (11.2 and 8.6 C-%, respectively).

Very differently, the processing of E-1 under analogous catalytic conditions was highly efficient, yielding 31.3 C-% of sorbitol at the end of the test (Run 2). This percentage exceeded by 7.4 points the number expected from the complete conversion of hexoses (i.e., glucose and cellobiose), denoting contributions from the depolymerisation of larger polysaccharides initially present in the effluent. Besides, approximately one-third of pentoses was transformed into xylitol (9.2 C-%), with another 8.1 C-% remaining unreacted. These results not only evidence the actual catalytic ability of the Ru/CNF but also illustrate the reactivity intrinsically different of xylose compared to that of glucose. The remaining xylose (7.3 C-%) probably underwent secondary off-path degradation routes, either into small molecular weight polyols via hydrogenolysis reactions of xylitol or by thermal decomposition. The formation of short-chain polyols could be noted to a certain degree (6.8 C-%), with erythritol and ethylene glycol being the most representative species (Barbaro et al., 2016; Delgado Arcaño et al., 2020). Fig. 3 summarises the main reaction routes involved in such transformations. In this case, no important formation of solid species by condensation/re-polymerisation was noted (only 1.7 C-%). This last percentage was added to the original insoluble fraction of 15.2 C-% in the product distribution representation. Overall, 75.5% of the carbon content of the starting stream (E-1) was quantified as different products, out of which 47.4 C-% corresponded to sugar alcohols.
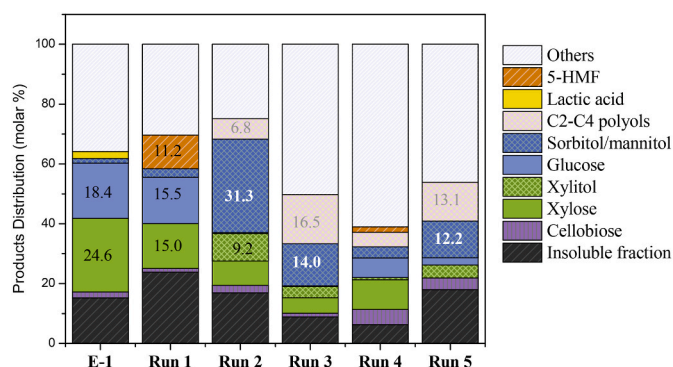

Fig. 2. Product distribution for E-1 downstream valorisation by hydrolytic hydrogenation under various experimental conditions. Run 1: Blank test (438 K, 5.0 MPa H_2, H_2O as a solvent), Run 3 (463 K, 5.0 MPa H_2, H_2O as a solvent), Run 4: (438 K, 1.5 MPa N_2, EtOH as a solvent), Run 5: (438 K, 5.0 MPa H_2, EtOH as a solvent).
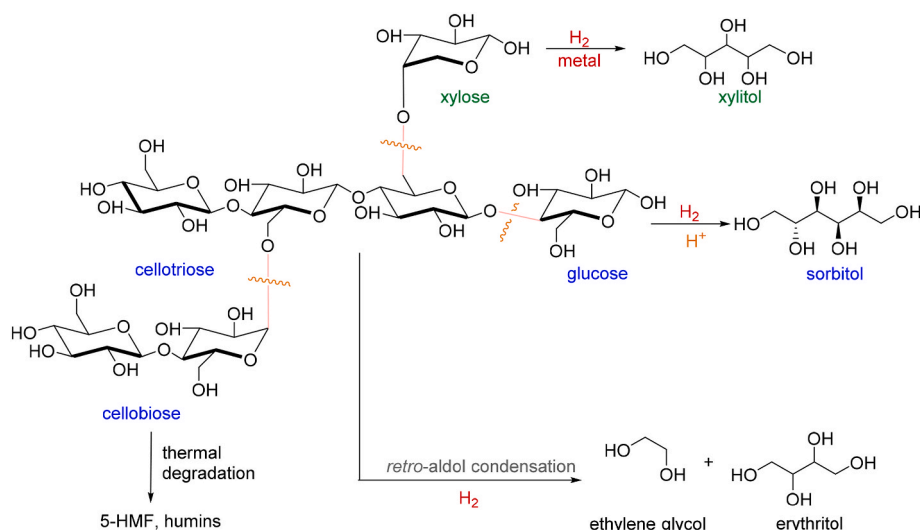
Fig. 3. Primary reaction routes involved in the catalytic hydrogenation of E1-A.

The reaction temperature is an essential factor in the hydrolytic hydrogenation of biomass since hydrolysis reactions occur to a shallow extent below 462 K in the absence of acidic catalysts (Frecha et al., 2021). This fact may underestimate the true potential of the stream E-1A to afford sugar alcohols at a low temperature (438 K) if the effluent contains long carbohydrate chains. The influence of the temperature was evaluated in a second run conducted at 463 K, including the insoluble fraction in the inlet effluent (Run 3), as it may contain non-soluble oligomers that could be depolymerised under harsher conditions. Indeed, the solid content recovered in the outlet effluent (6.3 C-%) revealed that part of the insoluble fraction could be dissolved. However, such a variation in the soluble-compounds concentration did not incur any enhancement in the hexitols production. Rather, it shifted the product distribution from C6-C5 alcohols to short molecular weight polyols (16.5 C-%), coming from the cleavage of the carbon chain. The strong impact of hydrogenolysis reactions after only 3 h at 463 K may be attributed to certain basic promotors such as N-containing proteins and other impurities derived from biomass (matrix effect). In general, the carbon balance closed at a lower extent (49.8 C-%) at 463 K, with only 14.0 C-% of sorbitol and 3.7 C-% of xylitol. The partial depolymerisation of large carbohydrates initially present in the solid fraction into water-soluble species can explain the decreases in the final amount of solid and carbon closure.

From a broader perspective, the hydrogen necessary for the hydrothermal hydrogenation of biomass can be procured either from molecular hydrogen gas or through the in-situ generation from hydrogen-donating species, governed by a catalytic transfer hydrogenation mechanism. This process can be illustrated as the combination of two fundamental reactions: the activation of organic hydrogen donor species and the reduction of sugars. As alcohols are commonly employed as hydrogen donors, and E-1 was primarily dissolved in ethanol, its direct application as a feedstock could potentially eliminate the need for an external source of hydrogen. (Scholz et al., 2015; García et al., 2020). In this context, an additional catalytic test (Run 4) was conducted by reacting E-1 under an autogenous pressure and an inert atmosphere (N_2) for 3 h at 437 K. Outside of minor amounts of sugar alcohols (3.7 C-% of sorbitol, 0.7 C-% of xylitol and 4.9 C-% of C2- C4 polyols), the development of hydrogenation reactions was negligible in the absence of a H_2 gas pressure, with most of the sugars being thermally degraded. The lack of an important conversion suggests that many other aspects related to the catalyst and process conditions, such as the presence of water as a co-solvent, the catalyst redox properties or even the cooperative effects between the metal and acid-base sites of the support, could be relevant to activate the alcohols on metallic surfaces and complete the catalytic

cycle (Shrotri et al., 2014; Kobayashi et al., 2011). This observation neglects the use of ethanol as a substitute molecular H_2, unless under the tested operating conditions. It is remarkable to note that the production of sugar alcohols in ethanol media remained unfavourable even when including an inlet H_2 pressure of 5.0 MPa (12.2 C-% of sorbitol and 4.3 C-% of xylitol, Run 5). The reason behind this finding could be ascribed to various viewpoints. On the one hand, the slight basic properties of ethanol may prompt hydrogenolysis pathways of C6 hexitols into lower molecular weight polyols, as evidenced by an increment in the C2-C4 polyols yield from 6.8% to 13.1%. On the other, and equally important, the absence of water prevented the hydrolysis of large carbohydrates into monosaccharides, which instead underwent alcoholysis reactions into ethyl glucosides.

Among various reaction conditions, the best-behaving catalytic system for hydrolytically hydrogenated E-1 is conducting the process in the aqueous phase under hydrogen gas (4.0 MPa) for 180 min at a mild temperature (438 K). Titled conditions afforded a carbon recovery as high as 75.5 C-%, with a remarkable yield in sugar alcohols (47.4 C-%). The excellent data substantially enhance the profitability of the nanocellulose production. From a purely economic standpoint, it is evident that the market value of sugar alcohols surpasses that of the non-valorised liquor, as demonstrated by the considerable price differential. Specifically, a syrup with a high concentration of xylose and glucose may have a wholesale price ranging from US $480–600/ton, depending on the content of reducing sugars. Additionally, it is worth noting that sorbitol is typically priced at US $650/ton, and the cost of xylitol may reach up to $3900/ton. (Taylor et al., 2015; Dávila et al., 2014).

3.3. MW-hydrolysate upgrading line

The liquid stream derived from the MW-assisted hydrothermal liquefaction of pre-treated almond hulls (E-2) comprises a broad spectrum of different species steaming from the decomposition of lignin, hemicellulose and amorphous cellulose that leach during this stage. The dissolution of lignin tends to yield oligomers and phenolic compounds, while carbohydrates mainly generate C5 and C6 saccharides. This effluent is a complex mixture of oxygenated compounds of different natures, characterised by a broad range of chemical species and concentrations, of which only 43.6% of the total C could be determined by HPLC and GC/MS-FID analysis (Table 2).

Such a heterogeneous composition, along with the low presence of individual constituents in the mixture, limits the selective conversion of this effluent to individual products, seemingly not appropriate for valorisation by hydrolytic hydrogenation. This fact could be experimentally

Table 2
Compositional analysis of E-2 by GC/MS-FID and HPLC.

Compound	Molecular Formula	Concentration (C-%)
Cellobiose	$C_{12}H_{22}O_{11}$	0.17
Galacturonic Acid	$C_6H_{10}O_7$	0.71
Arabinose/Rhamnose	$C_5H_{10}O_5$	1.03
Levoglucosan	$C_6H_{10}O_5$	1.38
5-HMF	$C_6H_6O_3$	0.97
Levulinic acid	$C_5H_8O_3$	4.30
Formic acid	CH_2O_2	2.38
Furfural	$C_5H_4O_2$	0.84
Lactic acid	$C_3H_6O_3$	3.12
Xylose	$C_5H_{10}O_5$	8.25
Acetic acid	CH_3COOH	9.09
Hydroxyacetone	$C_3H_6O_2$	2.92
Propanoic acid	$C_3H_6O_2$	0.13
2-Cyclopenten-1-one, 2-hydroxy-3,4 dimethyl	$C_7H_{10}O_2$	1.59
2-Cyclopenten-1-one, 2-hydroxy-3-methyl	$C_6H_8O_2$	4.00
2-Cyclopenten-1-one, 3-ethyl-2-hydroxy	$C_7H_{10}O_2$	1.43
3-hydroxypyridine	C_5H_5NO	1.29
Total		43.63

evidenced through a 3 h-treatment at 438 K in contact with the Ru/CNF catalyst and 5.0 MPa H_2 of pressure, in which only minor quantities of sorbitol and xylitol were determined by HPLC (2.5 and 0.4% in terms of carbon yield). Again, almost one-third of the xylose was unreacted (2.9 C-%), with up to 71.4% of the carbon content remaining without identification (Fig. S2 in ESI).

However, the relatively high content in organic carbon (0.96% on a C basis) renders this stream interesting for energy applications or as a chemical source. To recover and utilise these soluble molecules, the organic liquid extraction with various extracting agents was assessed, and the main results are summarised in Table 3. Initially, ethyl acetate was used as a solvent. After three extractions, it retained 18.7% of the carbon present in the aqueous phase, rendering an organic fraction (OP-A) in a mass yield of 8.5 ± 1.1% (Entry 1). A sequential methodology with chloroform and ethyl acetate, previously proposed by Ren et al. (2017), was also contemplated to increase the extraction efficiency. Notwithstanding, only a minimal improvement in the carbon recovery (19.8%) was noted upon this multi-step extraction, with also comparable values of yield (9.7% ± 1.4) based on a mass (Table 3, Entry 2). Therefore, the sole use of ethyl acetate could be enough to extract this phase for practical purposes. This also avoids the use of harmful solvents like chloroform, which is an essential consideration in the field of green chemistry.

The analysis of the organic extract by GC-MS (Table 4) showed one major peak area within their volatile portion, attributed to *N*-heterocyclic structures known as 3-hydroxypyridines. The relative distribution of these species is detailed in Fig. 4, including 3-hydroxypyridine as the main component (49.0–59.9 area %) and minute areas of 3-hydroxy-2-methylpyridine (0.9 area %) and 3-hydroxy-6-methylpyridine (0.9–2.2 area %). These compounds were likely originated from reactions between degradation products of sugars (i.e., furfurals generated through dehydration routes) and ammonia (issued from the deamination of hydrolysed proteins), in agreement with the literature (Madsen et al.,

Table 3
Chemical extraction of E-2.

Organic phase	Organic Solvent	Volumetric ratio (effluent: organic solvent)	Yield (wt. %)	Extraction efficiency (C-%)
OP-A	Ethyl acetate	(2:1)	8.5 ± 1.1	18.7
OP-B	Chloroform-Ethyl Acetate	(1:1) (2:1)	9.7 ± 1.4	19.8

Table 4
Chemical composition of organic extracts.

Chemical composition	Relative peak area (%)	
	OP-A	OP-B
3-hydroxy pyridines	52.0	61.3
Phenolic compounds	6.0	4.2
Acetic acid	10.5	9.8
2-Cyclopenten-1-one, 3-methyl-	6.4	5.6
5-hydroxymethylfurfural	5.8	5.9
Hydroxyacetone	2.4	n.d
Butanoic acid derivatives	1.1	1.6
Pentanoic acid derivatives	0.7	1.3
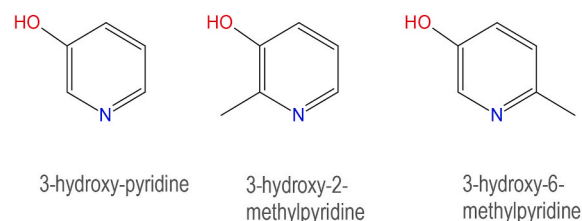
	3-hydroxy-pyridine	3-hydroxy-2-methylpyridine	3-hydroxy-6-methylpyridine
OP-A	49.0 %	0.9 %	2.2 %
OP-B	59.9 %	n.d	0.9 %

Fig. 4. Chemical structure and relative distribution of various 3-hydroxypyridine-derived compounds.

2017). Collectively, these species account for up to 52.0% of the area among the total substances identified by gas chromatography in OP-A. Smaller percentages of phenolics (6.0 area %), acetic acid (10.5 area %) and ketones (3-methyl-2-cyclopenten-1-one, 6.4 area %) were also detected. A rather similar composition was shown for OP-B, but owning a higher proportion of 3-hydroxypyridine (61.3 area %). Such unexpected selectivity towards specific extractable species could find utility in a certain niche of applications. In particular, 3-hydroxypyridine contains important structural entities for the synthesis of pharmaceutically relevant molecules used in medicine (vitamin B6, furopyridines, pterocellin A, pirbuterol) and agrochemicals as pesticides (trifloxysulfuron) (Sabot et al., 2012; Zhao et al., 2019; García Liñares et al., 2012; Yoshida et al., 2009).

It should be stressed, however, that these data are based on a semi-quantitative analysis where a high relative chromatographic area does not necessarily translate into a high concentration on a mass basis. Besides, it must be borne in mind that these liquids usually contain high-weight molecules undetectable by gas chromatography (Wildschut et al., 2009; Mohan et al., 2006). First estimations based on the elemental composition indicated that 3-hydroxypyridines may constitute up to 17.9 wt % of OP-A and 18.2 wt % of OP-B. The remainder of this fraction, mainly containing oligomeric species, could be a valuable starting material for energy and biofuel production. To more clearly disclose the potential, the fuel properties of the organic extracts were compared to a reference bio-oil sample, a dark brown liquid obtained from the MW-pyrolysis of almond hulls with a high heating value (*HHV*) of 28.7 MJ/kg. Table 5 presents a compilation of the data regarding the elemental analysis of the complete sample set. It was observed that the energy density of OP-A, which amounted to 22.7 MJ/kg, remained slightly lower than that of the bio-oil. This fact can be attributed to the comparatively higher proportion of oxygen moieties contained in OP-A, which constituted 35.5% as opposed to 24.2%. Furthermore, the oxygen-rich state of OP-B, which had a composition of 38.7%, further diminished its higher heating value to 21.6 MJ/kg. On the bright side, both OP-A and OP-B own more energy content than raw biomass (15.7 MJ/kg), which highlights the potential of this effluent for energy

Table 5
Elemental analysis and derived bio-oil properties.

Property	Bio-oil (MW-pyrolysis)	OP-A	OP-B
Elemental analysis (wt. %)			
C	64.7 ± 3.3	55.9 ± 0.6	52.1 ± 4.1
H	7.3 ± 0.5	5.9 ± 0.1	6.3 ± 0.1
N	3.7 ± 0.4	2.8 ± 0.2	2.8 ± 0.1
S	± 0.1	n.d	n.d
O[a]	24.2 ± 4.3	35.5 ± 0.6	38.7 ± 3.9
Molar H/C	1.36 ± 0.02	1.26 ± 0.02	1.46 ± 0.14
Molar O/C	0.28 ± 0.06	0.48 ± 0.01	0.56 ± 0.10
H/C_{eff} [b]	0.8	0.3	0.34
HHV (MJ/kg)	28.7 ± 2.2	22.7 ± 0.4	21.6 ± 1.7

n.d. = not detected.
[a] calculated by difference; [b] $H/C_{eff} = H/C - 2O/C$ on a molar basis (Ahmadi et al., 2017).

applications.

Together with the calorific value, the analysis of elemental compositions of these liquids gives useful insights into their chemical nature. An important descriptor in this field is the effective hydrogen to carbon molar ratio (H/C_{eff}) which defines the ratio between the hydrogen and carbon moles corrected by the oxygen content present as water. This ratio is nearly zero in sugars, nearly one for aromatics and equal to 2 in alkanes (Ahmadi et al., 2017). Accordingly, sugar-like structures are highly likely to be the most abundant chemical compounds being part of the OP samples, while the pyrolysis oil has an overall chemical composition resembling that of aromatic compounds.

The low HHVs and the huge amount of sugar-like substances impede the direct use of the organic products derived from the above stages as transportation fuels. This development is closely related to a series of detrimental characteristics inherited from the presence of oxygen entities (i.e., low energy density, immiscibility, high viscosity, corrosiveness, poor ignition and ageing properties) (Xiu and Shahbazi, 2012; Shan Ahamed et al., 2021). An up-and-coming methodology to improve the fuel and physicochemical properties of biomass-derived organic liquids to the industry standards is the catalytic hydrodeoxygenation (HDO). The process applies high temperatures (573–873 K) in the presence of hydrogen pressures and metal catalysts to eliminate oxygenates in the form of H_2O, CO and CO_2 through a variety of reactions, involving hydrogenation, hydrogenolysis, dehydration, decarbonylation and decarboxylation, hydrocracking or repolymerisation (Wildschut et al., 2009).

However, the hydrodeoxygenation of effluents with high levels of sugar-like compounds faces important drawbacks related to their tendency to form solid species via dehydration and polymerisation. To control the excessive coking during the HDO process, a previous stabilisation stage at low-severity conditions is often included, aimed at converting the most reactive chemical species into more stable derivatives. Carboxyl and carbonyl groups are typically converted to alcohols, while C=C linkages are saturated (Wildschut et al., 2009; French et al., 2010, 2011; Elliott et al., 1997; Venderbosch et al., 2010). A two-step strategy, widely adopted during the HDO of biomass-derived liquids, was suggested by Gagnon and Kaliaguine. According to this approach, the oil is initially stabilised at low temperatures (T < 553 K) and then subjected to a deeper deoxygenation at harsh conditions (623–873 K) to yield hydrocarbons (French et al., 2011; Han et al., 2019; Olarte et al., 2016; Gagnon and Kaliaguine, 1988). Common catalysts for this mild hydrotreatment include Ru, Pt and Pd, while Ru, Ni or sulfided CoMo catalysts are usually employed during the severe HDO stage (Han et al., 2019).

Given the demonstrated catalytic usefulness of Ru in the first HDO step (Wildschut et al., 2009, 2010; Xiu and Shahbazi, 2012; Venderbosch et al., 2010; Kim et al., 2019; Ruddy et al., 2014; Li et al., 2014b),

we have used the same Ru/CNF catalyst applied in the hydrolytic hydrogenation process of E-1 for the stabilisation of these organic effluents. The reaction was carried out for 60 min at 503 K and 4.0 MPa H_2 with ethanol as a solvent. The use of ethanol as the reaction medium not only avoids the need for subsequent extraction stages but also facilitates the dissolution of high molecular weight species due to its lower dielectric constant. Besides, the hydrogen solubility in ethanol is higher than in water (Ahmadi et al., 2016, 2017; Brand et al., 2013; Yang et al., 2016; Peng et al., 2009; Chen et al., 2013), which additionally promotes HDO reactions through a better gas-liquid mass transfer. The main properties of the hydrotreated samples derived from OP-A and OP-B are summarised in Tables 6 and 7. In terms of product recovery, only a minimal loss of yield was noted by coke formation (1.1–2.4 wt %) or gaseous products (0.98–1.1 wt % of CO_2). These results denoted that decarbonylation, decarboxylation or repolymerisation pathways did not occur substantially.

Changes in the chemical composition after the upgrading were outlined in Table 6. Again, 3-hydroxypyridines stand as the most abundant species within the volatile portion characterised by GC (based on the chromatographic area), with relative amounts of 51.1 and 67.6 area % for the hydrotreated OP-A and OP-B, respectively. Since these N-containing species were already present in the initial samples, their chemical stability is deduced during the mild catalytic hydrotreatment. The resistance permits their alternative recovery from the mixture before or after the hydrotreatment stage without important loss in yield. A second observation that can be deduced from these data is that most oligomeric structures could not break down into low molecular species detectable by GC, as attested by the minimal alteration in the chemical composition of the hydrotreated liquids compared to their untreated counterparts.

In addition to 3-hydroxypyridines, the hydrotreated organic phases owned relatively large quantities of organic acids, such as butanoic acid and their derivatives (21.7–29.7 area %) and pentanoic acids (5.1–2.7 area %). Two of the most interesting compounds that were identified within the first group are the diethyl ester of butanedioic acid (11.1–12.4 area %), so-called diethyl succinic acid (DES), and its alcohol analogue (2-hydroxybutanedioic acid, 1-ethyl ester, 10.6–17.3 area %). DES is an important intermediate for various industries, being used as a food additive, flavouring agent and solvent for pigments. Its physicochemical properties have also been explored as an additive for diesel fuels or as a fuel blending combined with a cetane number improver (Jenkins et al., 2017). In principle, the boiling point distances between these esters (~437 K) and 3-hydroxypiridines (~553 K) allow for an eventual separation of both species by simple distillation.

Overall, the disappearance of some oxygen-containing species, such as acetic acid and hydroxyacetone, along with an elemental oxygen reduction, suggests the effectiveness of mild hydrotreatment as a stabilisation method of both organic fractions (OP-A and OP-B). As a point of comparison, a bio-oil derived from the MW-pyrolysis was used as a reference feedstock. This bio-oil was initially composed of phenolic-like substances (67.9 area %), aromatics (naphthalenes, 13.4 area %) and ketones (3-methyl-2-cyclopenten-1-one, 3.5 area %). The stabilisation process dramatically increased the relative phenolics content to 89.8 area %, whereas the relative proportion of naphthalenes slightly decreased to 6.5 area %. Such changes occurred without significant

Table 6
Chemical composition of hydrotreated samples based on GC-detectable products.

Chemical composition	Hydrotreated OP-A	Hydrotreated OP-B
	Relative peak area (%)	
3-hydroxypyridines	51.1	67.6
Phenolic compounds	6.9	n.d.
Butanoic acid derivatives	21.7	29.7
Pentanoic acid derivatives	5.1	2.7

n.d = not detected.

Table 7
Chemical characterization of hydrotreated samples.

Property	Hydrotreated OP-A	Hydrotreated OP-B
Elemental analysis (wt. %)		
C	60.8 ± 0.1	58.2 ± 0.5
H	5.8 ± 0.1	5.5 ± 0.1
N	3.1 ± 0.1	3.0 ± 0.1
S	n.d	n.d
O[a]	30.3 ± 0.3	33.2 ± 0.5
Degree of deoxygenation (%)	14.6	14.1
H/C	1.15 ± 0.02	1.13 ± 0.04
O/C	0.37 ± 0.01	0.43 ± 0.01
H/C_{eff}	0.41	0.27
HHV (MJ/kg)	24.9 ± 0.2	23.3 ± 0.1

[a] calculated by difference.

variations in the molecular weight distributions (122.7 ± 0.2 g/mol for raw bio-oil and 120.4 ± 2.9 g/mol for the hydro-treated sample), neglecting the occurrence of severe chain cracking during this stage. The absence of cracking agrees with the results obtained during the HDO of OP-A and OP-B, mostly remaining in the oligomeric form.

Regarding the oxygen reduction, the Degree of Deoxygenation (*DOD*) of the organic phases ranged between 14.6 and 14.1% for OP-A and OP-B, in each case (Table 7), which means a mean decrease in the oxygen content of 5.3 ± 0.2 wt % and a concurrent improvement in their *HHVs* of around 1.9 ± 0.4 MJ/kg. OP-A shows the highest heating value (24.9 MJ/kg) and lower O/C ratio (0.37), followed by OP-B (23.3 MJ/kg, O/C = 0.43). A similar *DOD* value (16.9%) was determined for the MW-pyrolysis oil, which enhanced the *HHV* from 28.7 to 30.5 MJ/kg. In all the cases, the catalytic hydrotreatment in subcritical ethanol led to a product with an inferior O/C and reduced H/C values, pointing towards dehydration routes as the main reaction pathways (Ahmadi et al., 2017; Ardiyanti et al., 2015).

In summary, the information gathered from variations in the elemental and chemical compositions of the hydrotreated organic fractions indicates that this mild HDO treatment is a practical methodology for the first HDO stabilisation step, facilitating its storage and further processing into biofuels. Moreover, such a strategy allows for the simultaneous recovery of bioactive compounds (3-hydroxypyridines) and the synthesis of fuel additives (i.e., diethyl succinic acid), in addition to partially deoxygenated fuel intermediates (energy carriers).

3.4. Overall mass balances: a Sankey diagram with the best results attained in the valorisation of each effluent

On the blueprints, extracting sustainable cellulose nanomaterials as part of a fully integrated biorefinery seems more pragmatic than a single product-based preparation scheme. Fig. 5 displays major products and waste outputs as a Sankey diagram for the best results attained in the valorisation of each effluent. Herein, the width of the arrows is proportional to the flow quantity.

By this approach, it is possible to recuperate up to 7.9% of the original almond hulls weight as sugar alcohols after hydrolytically hydrogenating the effluent discharged during the feedstock pretreatment (E-1A), which constitutes around 40.7% of the hemicellulose (19.4%) initially present in the raw biomass. Assuming that the entire cellulose content (12.6%) was garnered as micro cellulose fibrils, it can be roughly estimated that nearly 64.1 wt % of the total carbohydrates, that is, the sum of cellulose and hemicellulose, was successfully transformed into marketable end products. Besides, the extraction with organic solvents enabled the valorisation of an additional 18.7% of the C present in the aqueous effluent released during the MW-hydrothermal treatment (E-2). The organic phase underwent a catalytic hydrotreatment process, leading to the formation of stable intermediates and fuel additives (DES). This process also involved a separation step between stages to isolate bioactive compounds, such as 3-hydroxypyridine, which accounted for 1.3 wt % of the final product. Collectively, it was possible to recover up to 36.7 wt % of the initial biomass as different co-products, which enhances the resource recovery of 40.6% as compared to the nanocellulose production without side streams valorisation (21.8 wt %).

4. Conclusions

The generation of defibrillated celluloses derived from almond hulls presents fresh prospects for business expansion stemming from a presently undervalued by-product. Nonetheless, to guarantee the economic and environmental viability of this procedure, the integration of all
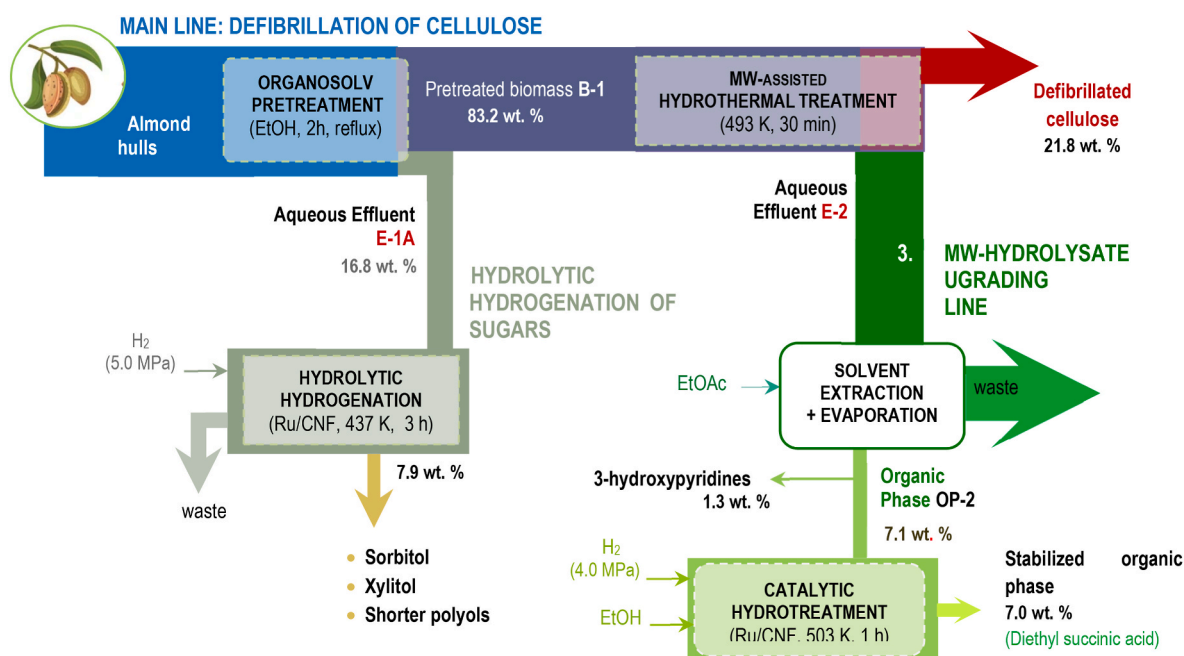

Fig. 5. Sankey diagram for defibrillated cellulose biorefinery concept from almond hulls.

accompanying processes within the overarching processing scheme is imperative. This can be achieved by leveraging the fractionation of feedstock and the potential synergies of resultant products. In this context, this work explored the catalytic valorisation of these streams within a novel biorefinery scheme for the first time. The sugar-rich aqueous effluent generated in the biomass preconditioning step can be effectively valorised by hydrolytic hydrogenation using a Ru/CNF catalyst at mild reaction conditions (i.e., 438–463 K and 5.0 MPa of H_2 for 3 h). This turned out to be an excellent modular process with a high selectivity towards sorbitol and xylitol (40.5 C-%) at 438 K or leading to a pool of various polyols (14.0 C-% of C6-hexitol, 3.7 C-% of C5-pentitol and 16.5 C-% of C2-C4 polyols) with further elevation on the temperature to 463 K. Additionally, soluble products present in the spent effluents derived from the MW-hydrothermal defibrillation could be readily collected and concentrated by conventional extraction, affording an organic phase with a maximum mass yield of 9.7% and remarkable content (18.2 wt %) in 3-hydroxypyridines. The rest of the organic phase could be a biofuel precursor upon a mild hydrodeoxygenation process (503 K, 1 h, 5.0 MPa H_2). This last process resulted in a stabilised organic oil with reduced oxygen content and a *HHV* between 23 and 35 MJ/kg, including fuel additives like diethyl succinic acid in their volatile fraction. This integrated and holistic approach represents a more competitive and advantageous use for nanocellulose production, gaining added value from previously discharged streams while contributing to the development of a zero-waste biorefinery unit for cellulose defibrillation.

CRediT authorship contribution statement

E. Frecha: Validation, and, Investigation, Writing – original draft. **J. Remón:** Conceptualization, and, Methodology, Writing – review & editing. **A.P. Sulaeman:** Validation, and, Investigation, Writing – review & editing. **A.S. Matharu:** Project administration, and, Funding acquisition, Supervision, Writing – review & editing. **I. Suelves:** Conceptualization, and, Methodology, Project administration, and, Funding acquisition, Supervision, Writing – review & editing. **J.L. Pinilla:** Conceptualization, and, Methodology, Project administration, and, Funding acquisition, Supervision, Writing – review & editing, All authors contributed to manuscript revision, read, and approved the submitted version.

Declaration of competing interest

The authors declare that they have no known competing financial interests or personal relationships that could have appeared to influence the work reported in this paper.

Data availability

Data will be made available on request.

Acknowledgements

Appendix A. Supplementary data

Supplementary data to this article can be found online at https://doi.org/10.1016/j.jclepro.2023.137582.

References

Ahmadi, S., Yuan, Z., Rohani, S., Xu, C., 2016. Catal. Today 269, 182–194.

Ahmadi, S., Reyhanitash, E., Yuan, Z., Rohani, S., Xu, C., 2017. Renew. Energy 114, 376–382.

Ardiyanti, A.R., Venderbosch, R., Yin, W., Heeres, H.J., 2015. RSC Energy and Environment Series 151–173.

Arevalo-Gallegos, A., Ahmad, Z., Asgher, M., Parra-Saldivar, R., Iqbal, H.M.N., 2017. Int. J. Biol. Macromol. 99, 308–318.

Barbaro, P., Liguori, F., Moreno-Marrodan, C., 2016. Green Chem. 18 (10), 2935–2940.

Bhaumik, P., Dhepe, P., 2015. Conversion of Biomass into Sugars. P., pp. 1–53.

Bozell, J.J., Landucci, I., 1993. Alternative Feedstocks Program Technical and Economic Assessment: Thermal/Chemical and Bioprocessing Components.

Bozell, J., Petersen, G., 2010. Green Chem. 12.

Brand, S., Susanti, R.F., Kim, S.K., Lee, H.-s., Kim, J., Sang, B.-I., 2013. Energy 59, 173–182.

Channiwala, S.A., Parikh, P.P., 2002. Fuel 81 (8), 1051–1063.

Chen, W., Luo, Z., Yang, Y., Li, G., Zhang, J., Dang, Q., 2013. Bioresources 8.

Cherubini, F., 2010. Energy Convers. Manag. 51 (7), 1412–1421.

Dávila, J.A., Hernández, V., Castro, E., Cardona, C.A., 2014. Bioresour. Technol. 161, 84–90.

de Melo, E.M., Clark, J.H., Matharu, A.S., 2017. Green Chem. 19 (14), 3408–3417.

Delgado Arcaño, Y., Valmaña García, O.D., Mandelli, D., Carvalho, W.A., Magalhães Pontes, L.A., 2020. Catal. Today 344, 2–14.

Dufresne, A., 2013. Mater. Today 16 (6), 220–227.

Elliott, D.C., Neuenschwander, G.G., 1997. Liquid fuels by low-severity hydrotreating of biocrude. In: Bridgwater, A.V., Boocock, D.G.B. (Eds.), Developments in Thermochemical Biomass Conversion: Volume 1/Volume 2. Springer Netherlands, Dordrecht, pp. 611–621.

Frecha, E., Torres, D., Pueyo, A., Suelves, I., Pinilla, J.L., 2019. Appl. Catal. Gen. 585, 117182.

Frecha, E., Torres, D., Suelves, I., Pinilla, J.L., 2021. Carbon 175, 429–439.

French, R.J., Hrdlicka, J., Baldwin, R., 2010. Environ. Prog. Sustain. Energy 29 (2), 142–150.

French, R.J., Stunkel, J., Baldwin, R.M., 2011. Energy Fuel. 25 (7), 3266–3274.

Gagnon, J., Kaliaguine, S., 1988. Ind. Eng. Chem. Res. 27 (10), 1783–1788.

Gao, Y., Xia, H., Sulaeman, A.P., de Melo, E.M., Dugmore, T.I.J., Matharu, A.S., 2019. ACS Sustain. Chem. Eng. 7 (13), 11861–11871.

Gao, Y., Ozel, M.Z., Dugmore, T., Sulaeman, A., Matharu, A.S., 2021a. J. Hazard Mater. 401, 123400.

Gao, Y., Remón, J., Matharu, A.S., 2021b. Green Chem. 23 (10), 3502–3525.

García, B., Moreno, J., Morales, G., Melero, J., Iglesias, J., 2020. Appl. Sci. 10, 1843.

García Liñares, G., Parraud, G., Labriola, C., Baldessari, A., 2012. Bioorg. Med. Chem. 20 (15), 4614–4624.

Geboers, J.A., Van de Vyver, S., Ooms, R., Op de Beeck, B., Jacobs, P.A., Sels, B.F., 2011. Catal. Sci. Technol. 1 (5), 714–726.

Han, Y., Gholizadeh, M., Tran, C.-C., Kaliaguine, S., Li, C.-Z., Olarte, M., Garcia-Perez, M., 2019. Fuel Process. Technol. 195, 106140.

Harini, K., Ramya, K., Sukumar, M., 2018. Carbohydr. Polym. 201, 329–339.

Hu, Z., Wen, Z., 2008. Biochem. Eng. J. 38 (3), 369–378.

Huber, G.W., Iborra, S., Corma, A., 2006. Chem. Rev. 106 (9), 4044–4098.

Iliyin, I., Purwaningsih, H., Irawadi, T., 2021. Jurnal Kimia Valensi 6, 169–176.

Jenkins, R.W., Bannister, C.D., Chuck, C.J., 2017. Proc. Inst. Mech. Eng. - Part D J. Automob. Eng. 231 (14), 1889–1899.

Jonoobi, M., Oladi, R., Davoudpour, Y., Oksman, K., Dufresne, A., Hamzeh, Y., Davoodi, R., 2015. Cellulose 22 (2), 935–969.

Jönsson, J., Pettersson, K., Berntsson, T., Harvey, S., 2013. Int. J. Energy Res. 37 (9), 1017–1035.

Kargarzadeh, H., Mariano, M., Gopakumar, D., Ahmad, I., Thomas, S., Dufresne, A., Huang, J., Lin, N., 2018. Cellulose 25 (4), 2151–2189.

Kim, S., Kwon, E.E., Kim, Y.T., Jung, S., Kim, H.J., Huber, G.W., Lee, J., 2019. Green Chem. 21 (14), 3715–3743.

Klemm, D., Kramer, F., Moritz, S., Lindström, T., Ankerfors, M., Gray, D., Dorris, A., 2011. Angew. Chem. Int. Ed. 50 (24), 5438–5466.

Kobayashi, H., Matsuhashi, H., Komanoya, T., Hara, K., Fukuoka, A., 2011. Chem. Commun. 47, 2366–2368.

Konwar, L.J., Kataki, R., Mikkola, J.P., Bordoloi, N., Saikia, R., Chutia, R., 2018. Side-streams from bioenergy and biorefinery complexes as a resource for circular bio-economy. Waste Biorefinery: Potential and Perspectives (Chapter 3).

Lavoine, N., Desloges, I., Dufresne, A., Bras, J., 2012. Carbohydr. Polym. 90 (2), 735–764.

Lee, H.V., Hamid, S.B.A., Zain, S.K., 2014. Sci. World J., 631013

Li, M., Cheng, Y.-L., Fu, N., Adhikari, B., Chen, X., 2014a. Int. J. Food Eng. 10, 427–436.

Li, Z., Kelkar, S., Raycraft, L., Garedew, M., Jackson, J.E., Miller, D.J., Saffron, C.M., 2014b. Green Chem. 16 (2), 844–852.

Li, Y., Liu, Y., Chen, W., Wang, Q., Liu, Y., Li, J., Yu, H., 2016. Green Chem. 18 (4), 1010–1018.

Luterbacher, J.S., Martin Alonso, D., Dumesic, J.A., 2014. Green Chem. 16 (12), 4816–4838.

Madsen, R.B., Bernberg, R.Z.K., Biller, P., Becker, J., Iversen, B.B., Glasius, M., 2017. Sustain. Energy Fuels 1 (4), 789–805.

Matharu, A.S., de Melo, E.M., 2018. ChemSusChem 11 (8), 1344–1353.

Mohan, D., Pittman, C.U., Steele, P.H., 2006. Energy Fuel. 20 (3), 848–889.

Moon, R.J., Martini, A., Nairn, J., Simonsen, J., Youngblood, J., 2011. Chem. Soc. Rev. 40 (7), 3941–3994.

Nagy Kim, D.H., Eckert, C.A., Liotta, C., Ragauskas, A., 2006. Ind. Biotechnol. 2, 55–56.

Nelson, K., Retsina, T., Iakovlev, M., van Heiningen, A., Deng, Y., Shatkin, J.A., Mulyadi, A., 2016. In: Madsen, L.D., Svedberg, E.B (Eds.), Materials Research for Manufacturing: an Industrial Perspective of Turning Materials into New Products. Springer International Publishing, pp. 267–302.

Novo, L.P., Bras, J., García, A., Belgacem, N., Curvelo, A.A.S., 2015. ACS Sustain. Chem. Eng. 3 (11), 2839–2846.

Novo, L.P., Bras, J., García, A., Belgacem, N., Curvelo, A.A.d.S., 2016. Ind. Crop. Prod. 93, 88–95.

Olarte, M.V., Zacher, A.H., Padmaperuma, A.B., Burton, S.D., Job, H.M., Lemmon, T.L., Swita, M.S., Rotness, L.J., Neuenschwander, G.N., Frye, J.G., Elliott, D.C., 2016. Top. Catal. 59 (1), 55–64.

Peng, J., Chen, P., Lou, H., Zheng, X., 2009. Bioresour. Technol. 100 (13), 3415–3418.

Reddy, N., Yang, Y., 2005. Trends Biotechnol. 23 (1), 22–27.

Remón, J., Latorre-Viu, J., Matharu, A., Pinilla, J.L., Suelves, I., 2020. Sci. Total Environ. 765, 142671.

Ren, S., Ye, X.P., Borole, A.P., 2017. J. Anal. Appl. Pyrol. 123, 30–39.

Ruddy, D.A., Schaidle, J.A., Ferrell Iii, J.R., Wang, J., Moens, L., Hensley, J.E., 2014. Green Chem. 16 (2), 454–490.

Sabot, C., Oueis, E., Brune, X., Renard, P.-Y., 2012. Chem. Commun. 48 (5), 768–770.

Scholz, D., Aellig, C., Mondelli, C., Pérez-Ramírez, J., 2015. ChemCatChem 7 (10), 1551–1558.

Shan Ahamed, T., Anto, S., Mathimani, T., Brindhadevi, K., Pugazhendhi, A., 2021. Fuel 287, 119329.

Sheikhi, A., 2019. Chapter 9 - emerging cellulose-based nanomaterials and nanocomposites. In: Karak, N. (Ed.), Nanomaterials and Polymer Nanocomposites. Elservier, pp. 307–351.

Shrotri, A., Kobayashi, H., Tanksale, A., Fukuoka, A., Beltramini, J., 2014. ChemCatChem 6 (5), 1349–1356.

Strain, H.H., 1937. J. Am. Chem. Soc. 59 (11), 2264–2266.

Sulaeman, A.P., Gao, Y., Dugmore, T., Remón, J., Matharu, A.S., 2021. Cellulose 28, 7687–7705.

Taylor, R., Nattrass, L., Alberts, G., Robson, P., Chudziak, C., Bauen, A., Libelli, I., Lotti, G., Prussi, M., Nistri, R., Chiaramonti, D., López-Contreras, A., Bos, H., Eggink, G., Springer, J., Bakker, R., van, R., 2015. From the Sugar Platform to Biofuels and Biochemicals. Final report for the European Commission Directorate-General Energy.

Venderbosch, R.H., Ardiyanti, A.R., Wildschut, J., Oasmaa, A., Heeres, H.J., 2010. J. Chem. Technol. Biotechnol. 85 (5), 674–686.

Wildschut, J., Mahfud, F.H., Venderbosch, R.H., Heeres, H.J., 2009. Ind. Eng. Chem. Res. 48 (23), 10324–10334.

Wildschut, J., Iqbal, M., Mahfud, F.H., Cabrera, I.M., Venderbosch, R.H., Heeres, H.J., 2010. Energy Environ. Sci. 3 (7), 962–970.

Wyman, C.E., 2003. Biotechnol. Prog. 19 (2), 254–262.

Xie, J., Hse, C.-Y., De Hoop, C.F., Hu, T., Qi, J., Shupe, T.F., 2016. Carbohydr. Polym. 151, 725–734.

Xie, H., Du, H., Yang, X., Si, C., 2018. International Journal of Polymer Science, 7923068.

Xiu, S., Shahbazi, A., 2012. Renew. Sustain. Energy Rev. 16 (7), 4406–4414.

Yang, T., Jie, Y., Li, B., Kai, X., Yan, Z., Li, R., 2016. Fuel Process. Technol. 148, 19–27.

Yoshida, K., Kawagoe, F., Hayashi, K., Horiuchi, S., Imamoto, T., Yanagisawa, A., 2009. Org. Lett. 11 (3), 515–518.

Zhang, Y.H.P., 2008. J. Ind. Microbiol. Biotechnol. 35 (5), 367–375.

Zhao, S., Hu, C., Guo, L., Li, K., Yu, H., 2019. Amb. Express 9 (1), 65, 65.

Zinge, C., Kandasubramanian, B., 2020. Eur. Polym. J. 133, 109758.